IEEE Photonics Journal
An IEEE Photonics Society Publication

Open Access

Performance Analysis of Hybrid FSO Systems Using FSO/RF-FSO Link Adaptation

Volume 10, Number 3, June 2018

Banibrata Bag
Akinchan Das
Imran Shafique Ansari
Aleš Prokeš
Chayanika Bose
Aniruddha Chandra

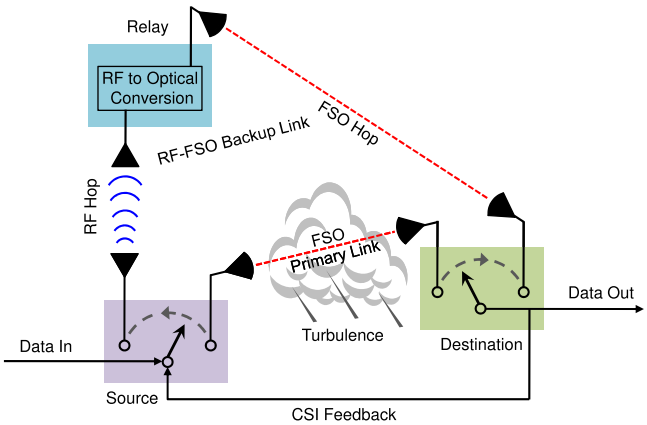

DOI: 10.1109/JPHOT.2018.2837356
1943-0655

IEEE photonics SOCIETY

IEEE

Performance Analysis of Hybrid FSO Systems Using FSO/RF-FSO Link Adaptation

Banibrata Bag,[1] **Akinchan Das**,[1] **Imran Shafique Ansari**,[2] **Aleš Prokeš**,[3] **Chayanika Bose**,[4] **and Aniruddha Chandra**[5]

[1]Haldia Institute of Technology, Haldia 721631, India
[2]Global College of Engineering and Technology, Muscat 2546, Oman
[3]Brno University of Technology, Brno 601 90, Czech Republic
[4]Jadavpur University, Kolkata 700032, India
[5]National Institute of Technology, Durgapur 713209, India

DOI:10.1109/JPHOT.2018.2837356

Manuscript received February 19, 2018; revised May 4, 2018; accepted May 12, 2018. Date of publication May 16, 2018; date of current version June 12, 2018. This work was supported by the Czech Science Foundation, Project No. 17-27068S Mobile channel analysis and modelling in millimeter wave band, and by the National Sustainability Program under grant LO1401 Interdisciplinary Research of Wireless Technologies. For the research, the infrastructure of the SIX Center was used. Corresponding authors: A. Chandra and A. Prokeš (e-mail: aniruddha.chandra@ieee.org; prokes@feec.vutbr.cz).

Abstract: Free-space optical (FSO) links are considered as cost-effective, noninvasive alternative to fiber optic cables for 5G cellular backhaul networking. For FSO-based backhaul networks, we propose an additional millimeter-wavelength (MMW) radio-frequency (RF)-FSO link, used as a backup. Uninterrupted and reliable network connection is possible by switching between primary FSO link and the secondary RF-FSO link; when the primary link is under atmospheric turbulence, the secondary link maintains connectivity as the MMW RF link exhibits complementary characteristics to atmospheric effects. In order to analytically assess the improvement, we also derive concise mathematical expressions for different performance metrics, such as outage probability, average bit error rate (BER), and capacity. Our results demonstrate that the FSO/RF-FSO topology performs better than a single FSO link in terms of outage probability and BER. The dual-hop mixed RF-FSO link is realized with an amplify and forward (AF) relay that adapts an average power scaling strategy. The irradiance fluctuations in the FSO links are modeled by gamma–gamma distribution, assuming strong atmospheric turbulence while it is assumed that the RF link experiences multipath Rayleigh fading. For switching between links, a single FSO threshold is considered first, followed by a dual FSO threshold to prevent unnecessary switching.

Index Terms: Free-space optics, 5G cellular backhaul, gamma-gamma fading, backup RF-FSO link, amplify-and-forward relay, link switching probability.

1. Introduction

The digital society of new generation is being accustomed to machine-to-machine (M2M) communication with high-speed Internet applications, and a demand for 1 Gbps connectivity per user is required to fulfil the dream of Internet-of-Things (IoT) in 5G networks. M2M communication in IoT would require communication between a huge number of connected devices. The challenge is to realize a backhaul infrastructure that supports a large node density and can carry an overwhelming amount of aggregated data. To extend the capacity, network operators are constantly diminishing

the size of the cells, but with every added base station the design of the backhaul network is becoming complex as well as expensive.

Free-space optical (FSO) communication is expected to play a vital role in 5G wireless networks. FSO links serve as a promising alternative to the conventional fiber optic cables utilized for backhaul links due to the ease of deployment, rapid setup time, and low maintenance cost [1], [2]. The downside of FSO is that it requires a clear line-of-sight (LOS) path and the propagation is highly influenced by the atmospheric turbulence [3]. Some hybrid paradigms incorporating both radio-frequency (RF) and FSO links have been proposed to combine the advantages of both links. In particular, FSO links offer much better data rates than RF links but suffer from atmospheric loss due to fog and scintillation whereas the RF link is a very good complement to FSO as RF is relatively insensitive to weather and it can penetrate fog easily. In our proposed FSO/RF-FSO scheme (see Fig. 1), the primary FSO link is utilized for better data rate when a clear LOS path exists, else a backup RF-FSO link is activated to sustain the connectivity. Under primary FSO link failure, this scheme provides a backup link to cope up with the weather conditions in hilly regions and industrial belts where dense fog, cloud, or smog often engulfs a part of the FSO transmission path.

1.1 Prior Work

While the idea of transmitting RF signals over FSO links in cellular mobile backhauls has been around the corner for quite some time [4], the network architectures proposing a combination of RF and FSO links are relatively new [5]. The proposed combinations are either *serial* where the middle node (relay node) of the cascaded link is utilized for RF-optical conversion [6] or *parallel* where a pair of RF and FSO links connects two network nodes to improve reliability [7].

The serial RF-FSO combination have been addressed in [8]–[10] where analytical expressions for amount of fading, outage probability, bit/ symbol error rate, and ergodic capacity have been derived. On the other hand, the parallel RF/FSO combination are considered in [11]–[13] where novel coding schemes are proposed for switching between RF and FSO paths.

Again, for channel characterization, different statistical models have been prescribed for both part of the links as RF and FSO links experience different atmospheric perturbations. For the RF link, Rayleigh [14], Ricean [15], Nakagami-m [16], and generalized distributions [17] are proposed to model the multipath fading. For characterizing atmospheric turbulence induced fading in FSO links, log-normal distribution has been utilized for long [18], although the distribution is suitable for modeling only weak turbulence. Recent experimental studies indicate that for FSO channel modeling gamma-gamma distribution is the most preferable candidate as it can model weak, moderate, and strong atmospheric turbulence conditions [19], [20].

1.2 Contributions

In this paper:

- A hybrid FSO/RF-FSO transmission scheme is presented to increase the availability and reliability of next generation cellular backhaul networks. To the best of our knowledge, analysis of performance metrics for a backhaul system where the primary FSO backhaul link is augmented with a serial RF-FSO backup link, has not been reported in the open literature so far. The proposed system is different from a hybrid RF/RF-FSO implementation [21][1] where the mobile users communicate with the respective base station via a RF or a RF-FSO link.
- By modeling the RF fading and atmospheric turbulence induced FSO fading with Rayleigh and gamma-gamma statistics, respectively, we derive analytical expressions for outage probability, average bit-error rate (BER), and ergodic capacity.
- The derived mathematical expressions for different performance metrics are presented in terms of Meijer's G-functions that can be accurately and easily computed using MATLAB or Wolfram Mathematica.

[1]This paper was co-authored by one of the current authors.

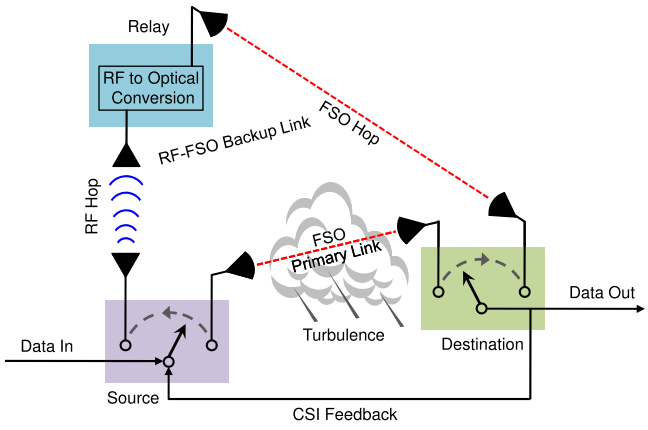

Fig. 1. Dual-hop mixed RF-FSO backup link with source-to-relay RF link and relay-to-destination FSO link.

- Two different link switching strategies are examined - a single FSO threshold scheme which offers simplicity in transceiver design, and a dual FSO threshold scheme that prevents unnecessary switching between primary FSO link and backup mixed RF-FSO link.
- All the mathematical analyses are verified through Monte Carlo simulations.

1.3 Organisation

The rest of this paper is structured as follows. Section II describes the proposed system model followed by statistical channel modeling of the primary FSO link and the backup RF-FSO link. Section III describes the link switching operation in Algorithm-1 under single FSO threshold scheme and presents analytical framework for calculation of outage probability, average BER, and ergodic capacity. The link switching operation for dual FSO threshold scheme is given in Algorithm-2 in Section IV followed by calculation of all the above-mentioned performance metrics under the dual threshold scheme. Both these sections contain the respective plots of numerical results as well. Finally, Section V concludes the paper with a brief summary and mentions possible directions to extend the current work.

2. System Configuration and Channel Model

In our proposed hybrid FSO/RF-FSO system, the FSO link works in parallel with a mixed RF-FSO link,[2] as the one depicted in Fig. 1. The source (S) contains an RF transmitter in addition to the regular FSO transmitter. The relay (R) is capable of receiving RF signal and subsequent RF-FSO conversion. At destination (D), there are two distinct optical receivers present; one for receiving data via S-D link and another for receiving the data through the relay, i.e. via S-R-D link.

The channel state information (CSI) about the primary FSO link is sent from D to S via a feedback path. If the primary FSO link is obscured due to atmospheric turbulence, S switches from FSO to RF transmission and notify D to switch to the receiver aligned with R. At regular intervals, S transmits a pilot signal through primary FSO link to gauge the turbulence condition. If the link quality meets the desired service level, D confirms it by sending a feedback, and the primary FSO link is re-activated.

[2]For a typical urban cellular backhaul application, the relay may be put on rooftops or it can be an unmanned aerial vehicle (UAV) node [2] placed at a suitable position to avoid the turbulence effect near the transmitter, to optimize energy consumption and to improve quality of service (QoS). Alternatively, the relay node may be just another regular transmitter with added RF-FSO conversion capability, i.e. all the transmitters can have an additional RF transceiver and an RF to FSO converter to realize this backup link concept.

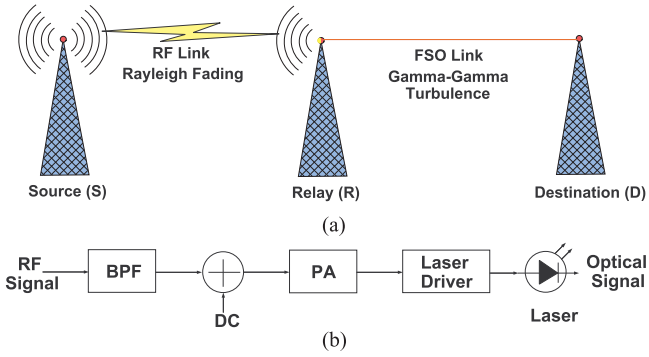

Fig. 2. (a) Dual-hop backup RF-FSO link with *S-R* RF hop and *R-D* FSO hop. (b) Block diagram of RF to optical converter implemented at *R* [14].

2.1 Modeling the Primary FSO Link

The probability density function (PDF) of the received instantaneous electrical signal to noise ratio (SNR) of the *S-D* link, $\xi_{fso} = (\eta I)^2 / N_0$, follows gamma-gamma distribution [22]

$$f_{\xi_{fso}}(\xi_{fso}) = \frac{(\alpha_t\beta_t)^{\frac{\alpha_t+\beta_t}{2}}}{\Gamma(\alpha_t)\Gamma(\beta_t)\sqrt{\xi_{fso}\bar{\xi}_{fso}}} \left(\sqrt{\frac{\xi_{fso}}{\bar{\xi}_{fso}}}\right)^{\frac{\alpha_t+\beta_t}{2}-1} K_{\alpha_t-\beta_t}\left(2\sqrt{\alpha_t\beta_t\sqrt{\frac{\xi_{fso}}{\bar{\xi}_{fso}}}}\right); \xi_{fso} \geq 0, \tag{1}$$

having an average electrical SNR of $\bar{\xi}_{fso} = (\eta \bar{I})^2 / N_0$, where η is the photo-current conversion ratio of the receiver, I is the received light intensity, N_0 is the one-sided power spectral density of additive white Gaussian noise (AWGN), and the operator $(\bar{\cdot})$ denotes mean value. The coefficients, α_t and β_t, are the effective number of small- and large-scale eddies of scattering environment [23], and together define the scintillation index, $SI = 1/\alpha_t + 1/\beta_t + 1/(\alpha_t\beta_t)$, utilized for measuring the optical intensity variation by atmospheric turbulence. Further, in (1), $\Gamma(\cdot)$ is the Gamma function and $K_v(\cdot)$ is the modified Bessel function of second kind of order v.

The cumulative distribution function (CDF) of electrical SNR, $F_{\xi_{fso}}(\xi_{fso})$, is found by using [24, eq. (8.4.23.1)] and integrating the PDF in (1) as

$$F_{\xi_{fso}}(\xi_{fso}) = \frac{(\alpha_t\beta_t)^{\frac{\alpha_t+\beta_t}{2}}}{2\Gamma(\alpha_t)\Gamma(\beta_t)\bar{\xi}_{fso}^{\tau_1}} \int_0^{\xi_{th}^{fso}} \xi_{fso}^{\tau_1-1} G_{0\,2}^{2\,0}\left[\alpha_t\beta_t\sqrt{\frac{\xi_{fso}}{\bar{\xi}_{fso}}}\,\middle|\, \begin{matrix} \frac{\alpha_t-\beta_t}{2} & \frac{\beta_t-\alpha_t}{2} \end{matrix}\right] d\xi_{fso}. \tag{2}$$

where $\tau_1 = (\alpha_t + \beta_t)/4$. Now, utilizing [25, eq. (26)], the above equation may be expressed as

$$F_{\xi_{fso}}(\xi_{fso}) = \frac{(\alpha_t\beta_t)^{\frac{\alpha_t+\beta_t}{2}}}{\Gamma(\alpha_t)\Gamma(\beta_t)\bar{\xi}_{fso}^{\tau_1}} \xi_{fso}^{\frac{\beta_t+\alpha_t}{4}} G_{1\,3}^{2\,1}\left[\alpha_t\beta_t\sqrt{\frac{\xi_{fso}}{\bar{\xi}_{fso}}}\,\middle|\, \begin{matrix} 1-\frac{\alpha_t+\beta_t}{2} \\ \frac{\alpha_t-\beta_t}{2} \quad \frac{\beta_t-\alpha_t}{2} \quad -\frac{\alpha_t+\beta_t}{2} \end{matrix}\right]. \tag{3}$$

2.2 Modeling the Backup RF-FSO Link

During primary link failure, *S* communicates with *D* via intermediate relay, *R*, using the backup *S-R-D* link. We have considered an average power scaling (APS) based fixed-gain amplify-and-forward (AF) type relay, as it is suitable for low budget relay based applications [26].

The *S-R* link can be characterized with Rayleigh fading whereas, assuming moderate to strong atmospheric turbulence, the *R-D* FSO link perturbations may be described by gamma-gamma distribution, as demonstrated in Fig. 2. The RF to FSO conversion is realized with a Mach-Zehnder modulator (MZM). The converter at the relay accepts RF signals from the source antenna and after conversion, the relay's optical transmitter sends an optical signal to the photo detector at the destination node lens.

If the instantaneous received electrical SNR for *S-R* and *R-D* links are denoted with ξ_{rf} and ξ_{fso}, respectively, the equivalent end-to-end instantaneous electrical SNR for an APS-AF relay is given by $\xi_{mix} = \xi_{rf}\xi_{fso}/(g_r + \xi_{fso})$ [27, eq. (6)], where the relay gain is $g_r = (1 + 1/N_0)$. As per our model, the *S-R* link experiences Rayleigh fading and the PDF of immediate SNR can be expressed as [28]

$$f_{\xi_{rf}}(\xi_{rf}) = \left(1/\bar{\xi}_{rf}\right) \exp\left(-\xi_{rf}/\bar{\xi}_{rf}\right);\ \xi_{rf} \geq 0, \tag{4}$$

where $\bar{\xi}_{rf}$ is the average SNR. The PDF of instantaneous electrical SNR of the *R-D* link follows gamma-gamma distribution as expressed in (1).

The CDF of end-to-end electrical SNR, $F_{\xi_{mix}}(\xi_{mix})$, is derived by integrating the conditional density over the whole range of ξ_{fso} using [24, eq. (2.24.3.1)], resulting in a closed-form expression

$$F_{\xi_{mix}}(\xi_{mix}) = 1 - \mathcal{K}_1 \exp\left(-\xi_{mix}/\bar{\xi}_{mix}\right) \xi_{mix}^{\tau_1} G_{0\ 5}^{5\ 0}\left[\omega\xi_{mix}\middle|_{\mathcal{P}}^{-}\right], \tag{5}$$

where $\mathcal{K}_1 = \frac{(\alpha_t\beta_t)^{\frac{\alpha_t+\beta_t}{2}}\left(g_r/\bar{\xi}_{rf}\right)^{\tau_1}}{4\pi\Gamma(\alpha_t)\Gamma(\beta_t)\left(\bar{\xi}_{fso}\right)^{\tau_1}}$, $\omega = \frac{\alpha_t^2\beta_t^2 g_r}{16\bar{\xi}_{rf}\bar{\xi}_{fso}}$, $\mathcal{P} \in \left\{\frac{\alpha_t-\beta_t}{4}, \frac{\alpha_t-\beta_t+2}{4}, \frac{\beta_t-\alpha_t}{4}, \frac{\beta_t-\alpha_t+2}{4}, -\tau_1\right\}$, and $G_{p\ q}^{m\ n}\left[z\middle|^{(a_p)}_{(b_q)}\right]$ is the Meijer's G-function [24, eq. (8.2.1)].

Further, differentiating (5) using [24, eq. (8.2.2.30)], the corresponding PDF is obtained as

$$\begin{aligned} f_{\xi_{mix}}(\xi_{mix}) = {} & \mathcal{K}_1 \exp\left(-\xi_{mix}/\bar{\xi}_{mix}\right) \xi_{mix}^{\tau_1-1} G_{1\ 6}^{6\ 0}\left[\omega\xi_{mix}\middle|^{-\tau_1}_{1-\tau_1,\mathcal{P}}\right] \\ & + \left(\mathcal{K}_1/\bar{\xi}_{mix}\right) \exp\left(-\xi_{mix}/\bar{\xi}_{mix}\right) \xi_{mix}^{\tau_1} G_{0\ 5}^{5\ 0}\left[\omega\xi_{mix}\middle|^{-}_{\mathcal{P}}\right]. \end{aligned} \tag{6}$$

3. Single FSO Threshold Scheme

Quality of the high speed primary FSO link (PL) is estimated by checking the signal level at *D* at frequent intervals. When the received signal level falls below a certain threshold, *D* sends this feedback to *S* so that an adaptive algorithm can determine the appropriate transmission path for further data transmission. Under the single threshold scheme, *S* automatically switches over to the RF-FSO secondary link (SL) if SNR falls below a certain fixed FSO threshold, ξ_{th}^{fso}, or falls into outage if the qualities of either of the RF or FSO link of mixed RF-FSO transmission path also falls below a certain common threshold, ξ_{th}^{mix} [11].

3.1 Link Switching Operation

The transmission path variable X at time $\mathcal{T}$ is selected as per Algorithm 1 described next.

3.2 Outage Probability Analysis

An outage occurs when both primary *S-D* link and secondary *S-R-D* link are down as the SNRs do not meet the respective threshold levels. The outage probability is thus

$$P_{out}^{(1)} = P_{out}^{fso(PL)}\left(\xi_{th}^{fso}\right) P_{out}^{mix}\left(\xi_{th}^{mix}\right), \tag{7}$$

where $P_{out}^{fso(PL)}$ is the outage probability of the primary FSO *S-D* link and P_{out}^{mix} is the outage probability of the secondary RF-FSO *S-R-D* link. The thresholds act as minimum SNR values above which the links can guarantee a specific QoS.

From (3) it is easy to find that $P_{out}^{fso(PL)}(\xi_{th}^{fso}) = F_{\xi_{fso}}(\xi_{th}^{fso})$, i.e.

$$P_{out}^{fso(PL)}\left(\xi_{th}^{fso}\right) = \frac{(\alpha_t\beta_t)^{\frac{\alpha_t+\beta_t}{2}}}{\Gamma(\alpha_t)\Gamma(\beta_t)\bar{\xi}_{fso}^{\tau_1}} \xi_{th}^{fso\ \frac{\beta_t+\alpha_t}{4}} G_{1\ 3}^{2\ 1}\left[\alpha_t\beta_t\sqrt{\xi_{th}^{fso}/\bar{\xi}_{fso}}\middle|^{1-\frac{\alpha_t+\beta_t}{2}}_{\frac{\alpha_t-\beta_t}{2}\ \frac{\beta_t-\alpha_t}{2}\ -\frac{\alpha_t+\beta_t}{2}}\right]. \tag{8}$$

Algorithm 1: Link Switching for Single FSO Threshold.

if $\xi_{fso}^{PL} \geq \xi_{th}^{fso}$ **then**
  $X_{\mathcal{T}} \leftarrow FSO$
else
  if $\left(\xi_{rf} \geq \xi_{th}^{mix}\right) \wedge \left(\xi_{fso}^{SL} \geq \xi_{th}^{mix}\right)$ **then**
    $X_{\mathcal{T}} \leftarrow RF\text{-}FSO$
  else
    Transmission suspended / Outage occurred
  end if
end if

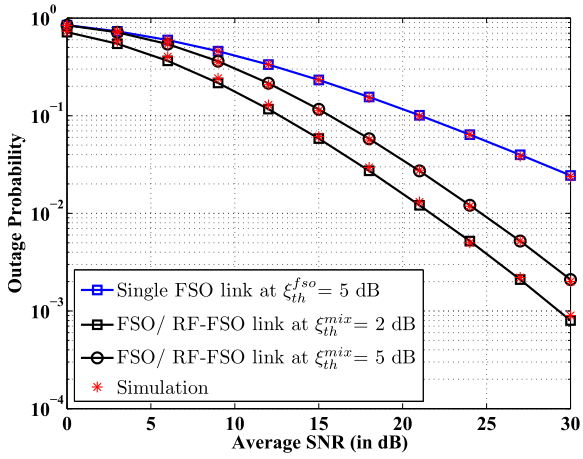

Fig. 3. Outage probability with single FSO threshold.

Similarly, the outage probability of the secondary RF-FSO link, $P_{out}(\xi_{th}^{mix}) = F_{\xi_{mix}}(\xi_{th}^{mix})$, is derived from (5) as

$$P_{out}^{mix}(\xi_{th}^{mix}) = 1 - \mathcal{K}_1 \exp\left(-\xi_{th}^{mix}/\bar{\xi}_{mix}\right) \xi_{th}^{mix\,\tau_1} G_{0\,5}^{5\,0}\left[\omega \xi_{th}^{mix}\Big|_{\mathcal{P}}^{-}\right]. \tag{9}$$

In Fig. 3, the numerical values obtained from the expressions developed for the outage probability are plotted and validated by Monte-Carlo simulations.[3] It may be seen that for an outage threshold of 5 dB, the outage probability is reduced by an order for an average electrical SNR of 30 dB, when we replace a single FSO link (blue line with square markers) with the proposed hybrid FSO/RF-FSO setup (black line with circle markers).

3.3 Average BER Analysis

During non-outage period, any one link can be active at any given instance. Therefore, three distinct scenarios should be considered for calculating the average BER. Extending the basic formulation

[3]We consider a fixed set of turbulence parameters, $(\alpha_t, \beta_t) = (5.07, 1.53)$, for the plot. Also, the average SNR per hop and the threshold SNR values are considered to be identical across all the branches, i.e. $\bar{\xi}_{rf} = \bar{\xi}_{fso}^{(SL)} = \bar{\xi}_{mix} = \bar{\xi}_{fso}^{(PL)}$ and $\xi_{th}^{rf} = \xi_{th}^{fso(SL)} = \xi_{th}^{mix} = \xi_{th}^{fso(PL)}$. These system parameters are used throughout for all the subsequent plots unless otherwise stated.

presented in [11], the average BER during the non-outage period can be expressed as

$$BER^{(1)} = \frac{B^{fso}\left(\xi_{th}^{fso}\right)}{1-P_{out}^{(1)}} + \frac{P_{out}^{rf}\left(\xi_{th}^{mix}\right)B^{mix}\left(\xi_{th}^{mix}\right)}{1-P_{out}^{fso(PL)}\left(\xi_{th}^{fso}\right)} + \frac{P_{out}^{fso(SL)}\left(\xi_{th}^{mix}\right)B^{mix}\left(\xi_{th}^{mix}\right)}{\left(1-P_{out}^{(1)}\right)\left(1-P_{out}^{rf}\left(\xi_{th}^{mix}\right)\right)}, \tag{10}$$

where B^{fso} and B^{mix} are the average BER when PL and SL are active, respectively, while $P_{out}^{rf}\left(\xi_{th}^{mix}\right)$ and $P_{out}^{fso(SL)}$ are the outage probabilities of the *S-R* link and *R-D* link. The first term in (10) accounts for the situation when $\xi_{fso}^{PL} > \xi_{th}^{fso}$ rendering the PL active. The second and third terms denote BER when SL is active and when $\xi_{rf} < \xi_{th}^{mix}$ or when $\xi_{rf} > \xi_{th}^{mix}$ but $\xi_{fso}^{SL} < \xi_{th}^{mix}$.

If we assume on-off keying (OOK) modulation, the conditional error probability is given by $P(e|\xi) = (1/2)\text{erfc}\left(\sqrt{\xi/2}\right)$. The average BER when primary FSO link is active

$$B^{fso}\left(\xi_{th}^{fso}\right) = \int_{\xi_{th}^{fso}}^{\infty} P\left(e\middle|\xi_{fso}^{PL}\right) f_{\xi_{fso}}\left(\xi_{fso}^{PL}\right) \mathrm{d}\xi_{fso}^{PL}. \tag{11}$$

under OOK modulation is thus found by substituting (1) in (11) as

$$B^{fso}\left(\xi_{th}^{fso}\right) = \mathcal{K}_2 \int_{\xi_{th}^{fso}}^{\infty} \text{erfc}\left(\sqrt{\xi_{fso}^{PL}/2}\right)\left(\xi_{fso}^{PL}\right)^{\tau_1-1} G_{0\,2}^{2\,0}\left[\alpha_t\beta_t\sqrt{\xi_{fso}^{PL}/\bar{\xi}_{fso}^{PL}}\,\middle|\, \begin{matrix} \\ \frac{\alpha_t-\beta_t}{2}\ \frac{\beta_t-\alpha_t}{2} \end{matrix}\right] \mathrm{d}\xi_{fso}^{PL}, \tag{12}$$

where $\mathcal{K}_2 = (\alpha_t\beta_t)^{\frac{\alpha_t+\beta_t}{2}}\left[4\Gamma(\alpha_t)\Gamma(\beta_t)\left(\bar{\xi}_{fso}^{PL}\right)^{\tau_1}\right]$. After some mathematical manipulations, we may express the integral as, $B^{fso}\left(\xi_{th}^{fso}\right) = \mathcal{I}_1 - (\mathcal{I}_{2_a} + \mathcal{I}_{2_b})$, where (see Appendix A for derivations)

$$\mathcal{I}_1 = \frac{\mathcal{K}_2 \cdot 2^{\tau_1-1}}{\pi^{3/2}} G_{2\,5}^{4\,2}\left[\frac{(\alpha_t\beta_t)^2}{8\bar{\xi}_{fso}^{PL}}\middle|_{\mathcal{P}}^{1-\tau_1,\,1/2-\tau_1}\right], \tag{13}$$

$$\mathcal{I}_{2_a} = \frac{\mathcal{K}_2(\xi_{th}^{fso})^{\tau_1}}{3}\sum_{k=0}^{\infty}\frac{(-\xi_{th}^{fso}/2)^k}{k!} G_{1\,3}^{2\,1}\left[\alpha_t\beta_t\sqrt{\xi_{th}^{fso}/\bar{\xi}_{fso}^{PL}}\,\middle|\, \begin{matrix} 1-\frac{\alpha_t+\beta_t}{2}-2k \\ \frac{\alpha_t-\beta_t}{2}\ \frac{\beta_t-\alpha_t}{2}\ -\frac{\alpha_t+\beta_t}{2}-2k \end{matrix}\right], \tag{14}$$

and

$$\mathcal{I}_{2_b} = \mathcal{K}_2(\xi_{th}^{fso})^{\tau_1}\sum_{k=0}^{\infty}\frac{(-2\xi_{th}^{fso}/3)^k}{k!} G_{1\,3}^{2\,1}\left[\alpha_t\beta_t\sqrt{\xi_{th}^{fso}/\bar{\xi}_{fso}^{PL}}\,\middle|\, \begin{matrix} 1-\frac{\alpha_t+\beta_t}{2}-2k \\ \frac{\alpha_t-\beta_t}{2}\ \frac{\beta_t-\alpha_t}{2}\ -\frac{\alpha_t+\beta_t}{2}-2k \end{matrix}\right]. \tag{15}$$

The average BER when RF-FSO link is active

$$B^{mix}\left(\xi_{th}^{mix}\right) = \int_{\xi_{th}^{mix}}^{\infty} P\left(e\middle|\xi_{mix}\right) f_{\xi_{mix}}(\xi_{mix})\,\mathrm{d}\xi_{mix}. \tag{16}$$

can be expressed as a sum of four individual integrals, $B^{mix}\left(\xi_{th}^{mix}\right) = (\mathcal{I}_{3_a} + \mathcal{I}_{3_b}) + (\mathcal{I}_{4_a} + \mathcal{I}_{4_b})$, where (see Appendix B for derivations)

$$\mathcal{I}_{3_a} = \frac{\mathcal{K}_1}{12}\left(\frac{1}{\bar{\xi}_{mix}} + \frac{1}{2}\right)^{-\tau_1} G_{2\,6}^{6\,1}\left[\frac{\omega}{\frac{1}{\bar{\xi}_{mix}} + \frac{1}{2}}\middle|_{1-\tau_1\mathcal{P}}^{-\tau_1-\tau_1}\right] - \frac{\mathcal{K}_1}{12}\sum_{k=0}^{\infty}\frac{(-1)^k}{k!}\left(\frac{1}{\bar{\xi}_{mix}} + \frac{1}{2}\right)^{k} \xi_{mix}^{\tau_1+k} G_{2\,7}^{6\,1}\left[\omega\xi_{mix}\middle|_{1-\tau_1,\mathcal{P}-\tau_1-k}^{1-\tau_1-k-\tau_1}\right], \tag{17}$$

$$\mathcal{I}_{3_b} = \frac{\mathcal{K}_1}{4}\left(\frac{1}{\bar{\xi}_{mix}} + \frac{2}{3}\right)^{-\tau_1} G_{2\,6}^{6\,1}\left[\frac{\omega}{\frac{1}{\bar{\xi}_{mix}} + \frac{2}{3}}\middle|_{1-\tau_1\mathcal{P}}^{-\tau_1-\tau_1}\right] - \frac{\mathcal{K}_1}{4}\sum_{k=0}^{\infty}\frac{(-1)^k}{k!}\left(\frac{1}{\bar{\xi}_{mix}} + \frac{2}{3}\right)^{k} \xi_{mix}^{\tau_1+k} G_{2\,7}^{6\,1}\left[\omega\xi_{mix}\middle|_{1-\tau_1,\mathcal{P}-\tau_1-k}^{1-\tau_1-k-\tau_1}\right], \tag{18}$$

$$\mathcal{I}_{4_a} = \frac{\mathcal{K}_1}{12\bar{\xi}_{mix}}\left(\frac{1}{\bar{\xi}_{mix}} + \frac{1}{2}\right)^{-\tau_1-1} G_{1\,5}^{5\,1}\left[\frac{\omega}{\frac{1}{\bar{\xi}_{mix}} + \frac{1}{2}}\middle|_{\mathcal{P}}^{-\tau_1}\right] - \frac{\mathcal{K}_1}{12\bar{\xi}_{mix}}\sum_{k=0}^{\infty}\frac{(-1)^k}{k!}\left(\frac{1}{\bar{\xi}_{mix}} + \frac{1}{2}\right)^{k} \xi_{mix}^{\tau_1+k+1} G_{1\,6}^{5\,1}\left[\omega\xi_{mix}\middle|_{\mathcal{P}-\tau_1-k-1}^{-\tau_1-k}\right], \tag{19}$$

and

$$\mathcal{I}_{4_b} = \frac{\mathcal{K}_1}{4\bar{\xi}_{mix}}\left(\frac{1}{\bar{\xi}_{mix}} + \frac{2}{3}\right)^{-\tau_1-1} G_{1\,5}^{5\,1}\left[\frac{\omega}{\frac{1}{\bar{\xi}_{mix}} + \frac{2}{3}}\middle|_{\mathcal{P}}^{-\tau_1}\right] - \frac{\mathcal{K}_1}{4\bar{\xi}_{mix}}\sum_{k=0}^{\infty}\frac{(-1)^k}{k!}\left(\frac{1}{\bar{\xi}_{mix}} + \frac{2}{3}\right)^{k} \xi_{mix}^{\tau_1+k+1} G_{1\,6}^{5\,1}\left[\omega\xi_{mix}\middle|_{\mathcal{P}-\tau_1-k-1}^{-\tau_1-k}\right]. \tag{20}$$

We have computed all the terms in (10) except P_{out}^{rf}, which, by definition, is

$$P_{out}^{rf}\left(\xi_{th}^{rf}\right) = \int_0^{\xi_{th}^{rf}} f_{\xi_{rf}}(\xi_{rf})\mathrm{d}\xi_{rf}. \tag{21}$$

Placing (4) in (21) and utilizing the lower incomplete gamma function [29, eq. (8.350.1)] and [24, eq. (8.4.16.1)], we may write

$$P_{out}^{rf}\left(\xi_{th}^{rf}\right) = \gamma\left(1, \frac{\xi_{th}^{rf}}{\xi_{rf}}\right) = G_{1\,2}^{1\,1}\left[\frac{\xi_{th}^{rf}}{\xi_{rf}}\middle|_{10}^{1}\right]. \tag{22}$$

BER performance with single FSO threshold is demonstrated in Fig. 4. The improvement is clearly visible, for example, at a target BER of 10^{-2} and for a threshold value of 5 dB, the proposed setup (black line with square markers) achieves an electrical SNR gain of 15 dB over the single FSO link (blue line with diamond markers).

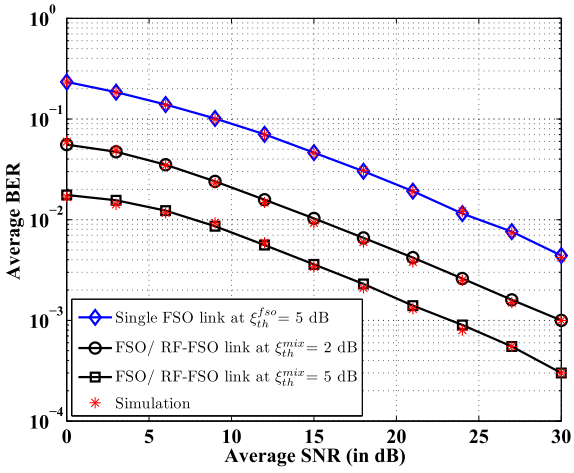

Fig. 4. Average BER with single FSO threshold.

3.4 Average Capacity Analysis

The average capacity of the FSO/RF-FSO system, when at least any one link remain active, can be computed according to Algorithm 1 as

$$C^{(1)} = C_{fso}^{PL}\left(\xi_{th}^{fso}\right) + P_{out}^{fso(PL)}\left(\xi_{th}^{fso}\right) C_{mix}\left(\xi_{th}^{mix}\right) + P_{out}^{rf}\left(\xi_{th}^{rf}\right)\left[1 - P_{out}^{fso(SL)}\left(\xi_{th}^{mix}\right)\right] C_{fso}^{SL}\left(\xi_{th}^{mix}\right), \tag{23}$$

where $P_{out}^{fso(PL)}\left(\xi_{th}^{fso}\right)$ and $P_{out}^{rf}\left(\xi_{th}^{mix}\right)$ are given by (8) and (22), respectively. When $\xi_{fso}^{PL} > \xi_{th}^{fso}$, PL is active, and $C_{fso}^{PL}\left(\xi_{th}^{fso}\right)$ is the average capacity, whereas, when $\xi_{fso}^{PL} < \xi_{th}^{fso}$, outage occurs at PL with probability $P_{out}^{fso(PL)}\left(\xi_{th}^{fso}\right)$, and capacity of the SL is $C_{mix}\left(\xi_{th}^{mix}\right)$. If $\xi_{rf} < \xi_{th}^{mix}$, outage occurs in *S-R* RF link with outage probability P_{out}^{rf}, but still it is possible that the *R-D* FSO link remains active; busy in transmitting some stored data in relay node with a capacity $C_{fso}^{SL}\left(\xi_{th}^{mix}\right)$. However, we should exclude the case $\xi_{fso}^{SL} < \xi_{th}^{mix}$, i.e. when outage occurs in the *R-D* FSO link, having a probability of $P_{out}^{fso(SL)}\left(\xi_{th}^{mix}\right)$.

The capacity term when PL is active,[4]

$$C_{fso}^{PL}\left(\xi_{th}^{fso}\right) = \int_{\xi_{th}^{fso}}^{\infty} \log_2\left(1+\xi_{fso}^{PL}\right) f_{\xi_{fso}}\left(\xi_{fso}^{PL}\right) \mathrm{d}\xi_{fso}^{PL}$$
$$= \frac{\mathcal{K}_1}{\ln(2)} \int_{\xi_{th}^{fso}}^{\infty} \ln\left(1+\xi_{fso}^{PL}\right)\left(\xi_{fso}^{PL}\right)^{\tau_1-1} G_{0\,2}^{2\,0}\left[\alpha_t\beta_t\sqrt{\frac{\xi_{fso}^{PL}}{\bar{\xi}_{fso}^{PL}}}\,\middle|\,\frac{\beta_t-\alpha_t}{2}-\frac{\beta_t-\alpha_t}{2}\right] \mathrm{d}\xi_{fso}^{PL}, \tag{24}$$

can be expressed as a difference, $C_{fso}^{PL}\left(\xi_{th}^{fso}\right) = \mathcal{I}_5 - \mathcal{I}_6$, where (see Appendix C for derivations)

$$\mathcal{I}_5 = \mathcal{K}_1/[2\pi\ln(2)]\, G_{2\,6}^{6\,1}\left[\alpha_t^2\beta_t^2/\left(16\bar{\xi}_{fso}^{PL}\right)\,\middle|_{\mathcal{P},-\tau_1}^{-\tau_1,1-\tau_1}\right], \tag{25}$$

and

$$\mathcal{I}_6 = \frac{2\mathcal{K}_1}{\ln(2)} \sum_{n=1}^{\infty} \frac{(-1)^{n+1}}{n!}\left(\xi_{th}^{fso}\right)^{\frac{\alpha_t\beta_t}{4}+n} G_{1\,3}^{2\,1}\left[\alpha_t\beta_t\sqrt{\xi_{th}^{fso}/\bar{\xi}_{fso}^{PL}}\,\middle|\,\frac{1-\frac{\beta_t+\alpha_t}{2}-2n}{\frac{\beta_t-\alpha_t}{2}\;\frac{\beta_t-\alpha_t}{2}\;-\frac{\beta_t-\alpha_t}{2}-2n}\right]. \tag{26}$$

[4]In strict sense, this capacity expression is valid for coherent FSO systems, but can be used as a bound for intensity modulation/direct detection (IM/DD) FSO systems if an exponential corrective term [30] is added.

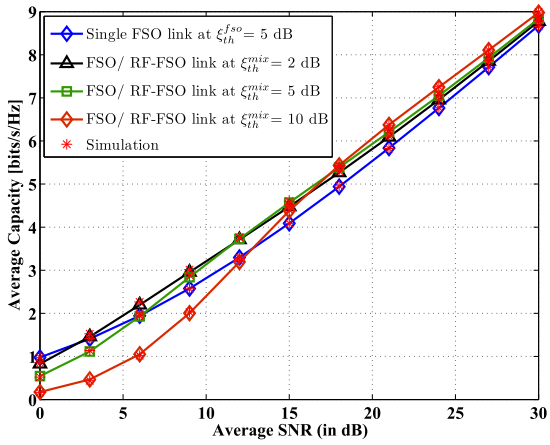

Fig. 5. Average capacity with single FSO threshold.

The term, $C_{fso}^{SL}\left(\xi_{th}^{mix}\right)$, may also be found in a similar way by replacing ξ_{th}^{fso} with ξ_{th}^{mix} in (24).

Furthermore, the average capacity when SL is active,

$$C_{mix}\left(\xi_{th}^{mix}\right) = \int_{\xi_{th}^{mix}}^{\infty} \log_2\left(1+\xi_{mix}\right) f_{\xi_{mix}}(\xi_{mix}) \mathrm{d}\xi_{mix}, \tag{27}$$

can be expressed as a combination of four individual integrals, $C_{mix}\left(\xi_{th}^{mix}\right) = (\mathcal{C}_1 - \mathcal{C}_2) + (\mathcal{C}_3 - \mathcal{C}_4)$, where (see Appendix D for derivations)

$$\mathcal{C}_1 = \frac{\mathcal{K}_1}{\ln(2)} \sum_{n=1}^{\infty} \frac{(-1)^{n+1}}{n\left(\bar{\xi}_{mix}\right)^{n\tau_1}} G_{2\,6}^{6\,1}\left[\omega\bar{\xi}_{mix}\middle|_{1-\tau_1\mathcal{P}}^{1-n-\tau_1-\tau_1}\right], \tag{28}$$

$$\mathcal{C}_2 = \frac{\mathcal{K}_1}{\ln(2)} \sum_{n=1}^{\infty} \frac{(-1)^{n+1}}{n} \sum_{k=0}^{\infty} \frac{(-1)^k}{k!} \left(\xi_{th}^{mix}\right)^{n+\tau_1+k} G_{2\,7}^{6\,1}\left[\omega\xi_{th}^{mix}\middle|_{1-\tau_1\mathcal{P}-n-\tau_1-k}^{1-n-\tau_1-k-\tau_1}\right], \tag{29}$$

$$\mathcal{C}_3 = \frac{\mathcal{K}_1}{\ln(2)} \sum_{n=1}^{\infty} \frac{(-1)^{\tau_1}}{n\left(\bar{\xi}_{mix}\right)^{(\tau_1+n+2)}} G_{1\,5}^{5\,1}\left[\omega\bar{\xi}_{mix}\middle|_{\mathcal{P}}^{-\tau_1-n}\right], \tag{30}$$

and

$$\mathcal{C}_4 = \frac{\mathcal{K}_1}{\ln(2)\,\bar{\xi}_{mix}} \sum_{n=1}^{\infty} \frac{(-1)^{n+1}}{n} \sum_{k=1}^{\infty} \frac{(-1)^k}{k!} \left(\xi_{th}^{mix}\right)^{\tau_1+n+k+1} G_{1\,6}^{5\,1}\left[\omega\xi_{th}^{mix}\middle|_{\mathcal{P}-\tau_1-n-k-1}^{-\tau_1-n-k}\right]. \tag{31}$$

Fig. 5 depicts the average capacity of the system with single FSO threshold. On utilizing the hybrid scheme, the average capacity of overall system increases, but this improvement occurs only after some cutoff SNR. The cutoff SNR increases with threshold SNR value.

4. Dual FSO Threshold Scheme

The single FSO threshold scheme presented in the previous section leads to continuous ON/OFF transitions between the PL and the SL, which can be reduced with dual FSO thresholds. In this scheme, the FSO PL remains in ON state as long as the SNR of the PL remains above a lower threshold level, $\xi_{th_{LB}}^{fso}$, failing which the PL switches to OFF state and the system switches to the RF-FSO SL for data transmission provided this link's SNR is above ξ_{th}^{mix}. The PL is switched back to ON state when the SNR exceeds $\xi_{th_{UB}}^{fso}$, where $\xi_{th_{UB}}^{fso} > \xi_{th_{LB}}^{fso}$.

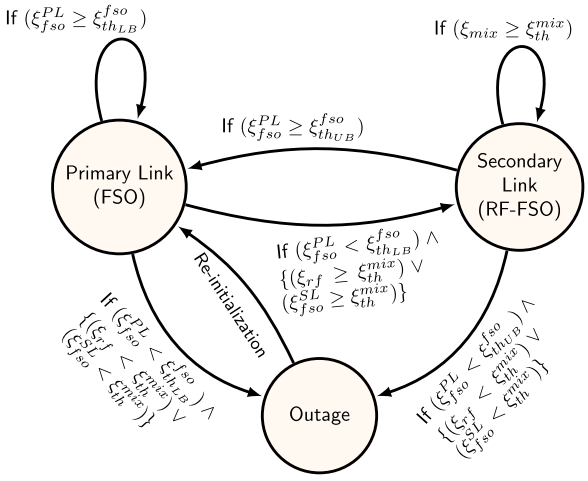

Fig. 6. State transition diagram with dual FSO threshold.

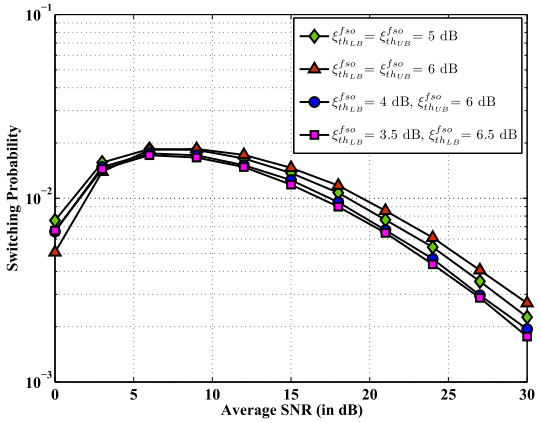

Fig. 7. Switching probability with single and dual FSO threshold.

Algorithm 2: Link Switching Algorithm for Dual FSO Threshold.

if $((X_{\mathcal{T}-1} = FSO) \wedge (\xi_{fso}^{PL} \geq \xi_{th_{LB}}^{fso})) \vee ((X_{\mathcal{T}-1} = RF\text{-}FSO) \wedge (\xi_{fso}^{PL} \geq \xi_{th_{UB}}^{fso}))$ **then**
  $X_{\mathcal{T}} \leftarrow FSO$
else
  if $\left(\xi_{rf} \geq \xi_{th}^{mix}\right) \wedge \left(\xi_{fso}^{SL} \geq \xi_{th}^{mix}\right)$ **then**
    $X_{\mathcal{T}} \leftarrow RF\text{-}FSO$
  else
    Transmission suspended / Outage occurred
  end if
end if

4.1 Link Switching Operation

In Algorithm 2, we describe the link switching operation under dual FSO threshold. Similar to Algorithm 1, $X_{\mathcal{T}}$ denotes the transmission path variable at time $\mathcal{T}$. The previous value of the variable, $X_{\mathcal{T}-1}$, is the value of the last selection that occurred in the previous switching instant $\mathcal{T}-1$. The switching operation of the system is depicted with a state transition diagram in Fig. 6.

When $\xi_{th_{UB}}^{fso} = \xi_{th_{LB}}^{fso}$, it is apparent that the system becomes identical to the one described in previous section. Fig. 7 shows that the switching probability is highest for such a case, and further,

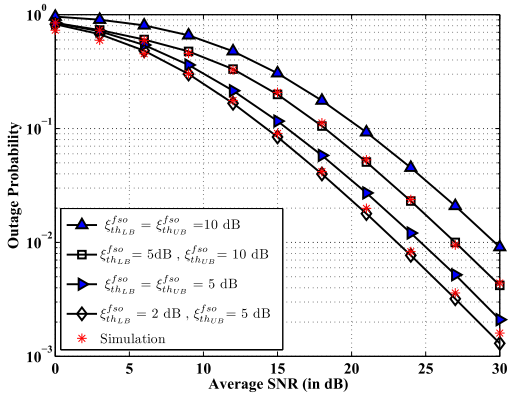

Fig. 8. Outage probability with single and dual FSO threshold.

the amount of switching is increases when this common threshold goes up. With dual threshold, the switching probability reduces, and as the gap between $\xi^{fso}_{th_{LB}}$ and $\xi^{fso}_{th_{UB}}$ widens (2 dB for blue circle markers, 3 dB for pink square markers), the switching lowers further as the system gets sufficient space to swing freely without switching to other link.

4.2 Outage Probability Analysis

An outage occurs when PL SNR is below $\xi^{fso}_{th_{LB}}$ and SL SNR is below ξ^{mix}_{th}. The corresponding probability can be calculated as

$$P^{(2)}_{out} = P^{fso(PL)}_{out_{Dual}}\left(\xi^{fso}_{th_{LB}}, \xi^{fso}_{th_{UB}}\right) P^{mix}_{out}\left(\xi^{mix}_{th}\right) = \left[P^{fso(PL)}_{out}\left(\xi^{fso}_{th_{LB}}\right) + \mathcal{P}_A \mathcal{P}_B\right] P^{mix}_{out}\left(\xi^{mix}_{th}\right), \tag{32}$$

where, $P^{fso(PL)}_{out_{Dual}}\left(\xi^{fso}_{th_{LB}}, \xi^{fso}_{th_{UB}}\right)$ is the probability that outage occurs in PL, $\mathcal{P}_A = P^{fso(PL)}_{out}\left(\xi^{fso}_{th_{UB}}\right) - P^{fso(PL)}_{out}\left(\xi^{fso}_{th_{LB}}\right)$, is the probability that the FSO link SNR lies between $\xi^{fso}_{th_{LB}}$ and $\xi^{fso}_{th_{UB}}$, and $\mathcal{P}_B = P^{fso(PL)}_{out}\left(\xi^{fso}_{th_{LB}}\right)\left[P^{fso(PL)}_{out}\left(\xi^{fso}_{th_{UB}}\right) + P^{fso(PL)}_{out}\left(\xi^{fso}_{th_{LB}}\right)\right]$, is the probability that the FSO link SNR previously lied below the lower bound $\xi^{fso}_{th_{LB}}$. With the help of above formulation and using the expressions derived for single FSO threshold scheme, it is straightforward to compute the outage probability for dual FSO threshold scheme.

In Fig. 8, we compare the outage probability with single and dual FSO threshold. When we set $\xi^{fso}_{th_{LB}}$ (say 2 dB) below the fixed threshold value (say 5 dB), while keeping $\xi^{fso}_{th_{UB}}$ at the same level as that of the fixed threshold (i.e. both at 5 dB), the outage probability reduces (compare the bottom two plots in Fig. 8). The performance gap is increased (compare the top two plots in Fig. 8) when the gap between upper and lower threshold increases.

4.3 Average BER Analysis

The expression of average bit error probability with OOK modulation of our considered system under dual FSO threshold scheme can be expressed as

$$BER^{(2)} = \frac{1}{1 - P^{(2)}_{out}}\left\{B^{fso}\left(\xi^{fso}_{th_{UB}}\right) + \frac{\left[B^{fso}\left(\xi^{fso}_{th_{LB}}\right) - B^{fso}\left(\xi^{fso}_{th_{UB}}\right)\right]\left[1 - P^{fso(PL)}_{out}\left(\xi^{fso}_{th_{UB}}\right)\right]}{1 - P^{fso(PL)}_{out}\left(\xi^{fso}_{th_{UB}}\right) + P^{fso(PL)}_{out}\left(\xi^{fso}_{th_{LB}}\right)}\right.$$
$$\left. + \frac{P^{rf}_{out}\left(\xi^{mix}_{th}\right) B^{mix}\left(\xi^{mix}_{th}\right)}{1 - P^{fso(SL)}_{out}\left(\xi^{mix}_{th}\right)} + \frac{P^{fso(SL)}_{out}\left(\xi^{mix}_{th}\right) B^{mix}\left(\xi^{mix}_{th}\right)}{1 - P^{rf}_{out}\left(\xi^{mix}_{th}\right)}\right\} + P^{(2)}_{out} B^{mix}\left(\xi^{mix}_{th}\right), \tag{33}$$

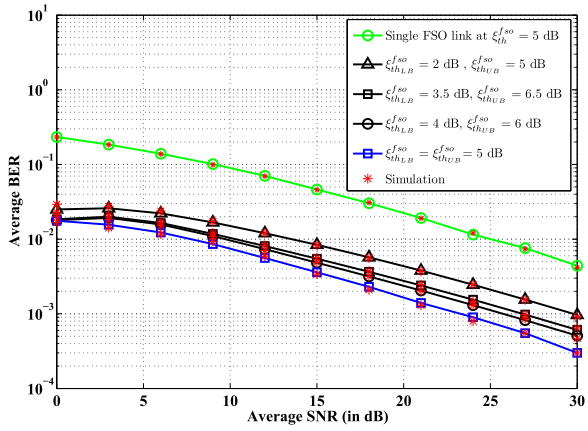

Fig. 9. Average BER with dual FSO threshold.

where B^{fso} and B^{mix} are as expressed in (12) and (16), the overall outage probability, $P_{out}^{(2)}$, is given by (32), while the other outage terms $P_{out}^{fso(PL)}$ (as well as $P_{out}^{fso(SL)}$) and P_{out}^{rf} may be computed from (8) and (22), respectively.

In (33), the first term represents the situation when $\xi_{fso}^{PL} \geq \xi_{th_{UB}}^{fso}$, PL is active, and error probability during non-outage period is given by $B^{fso}\left(\xi_{th_{UB}}^{fso}\right) / \left[1 - P_{out}^{(2)}\right]$. Similarly, the second term represents the situation, $\xi_{th_{LB}}^{fso} < \xi_{fso}^{PL} \leq \xi_{th_{LB}}^{fso}$. When $\xi_{fso}^{PL} < \xi_{th_{LB}}^{fso}$, SL becomes active and if $\{\xi_{rf}, \xi_{mix}\} \geq \xi_{th}^{mix}$, error for the SL would be $P_{out}^{(2)} B_{mix}\left(\xi_{th}^{mix}\right)$, which accounts for the last term in (33). The third and fourth term of (33), on the other hand, accounts for the cases when $\xi_{rf} < \xi_{th}^{mix}$ and when $\xi_{rf} > \xi_{th}^{mix}$ but $\xi_{fso}^{SL} < \xi_{th}^{mix}$, respectively.

Fig. 9 demonstrates variation of the average BER against the average electrical SNR with different combinations of dual FSO thresholds. When compared to the single FSO threshold at $\xi_{th}^{fso} = 5$ dB (blue line), the BER penalty is clearly visible. If $\xi_{th_{UB}}^{fso} = 5$ dB and $\xi_{th_{LB}}^{fso} = 2$ dB (black line with triangular markers), for a target BER of 10^{-3}, there is an SNR penalty of about 6 dB. This is because, when $\xi_{th_{LB}}^{fso} < \xi_{th}^{fso} = \xi_{th_{UB}}^{fso}$, the PL remains active due to dual thresholds instead of switching to a better quality SL which would have happened if there was only a single threshold. Nevertheless, the system's BER performance is still improved compared to single FSO link setup (green line).

4.4 Average Capacity Analysis

Considering the dual FSO threshold scheme, the expression for the average capacity of such a system can be expressed as

$$\begin{aligned} C^{(2)} &= C_{fso}^{PL}\left(\xi_{th_{UB}}^{fso}\right) \\ &+ \left[C_{fso}^{PL}\left(\xi_{th_{LB}}^{fso}\right) - C_{fso}^{PL}\left(\xi_{th_{UB}}^{fso}\right)\right]\left[\frac{1 - P_{out}^{fso(PL)}\left(\xi_{th_{UB}}^{fso}\right)}{1 - P_{out}^{fso(PL)}\left(\xi_{th_{UB}}^{fso}\right) + P_{out}^{fso(PL)}\left(\xi_{th_{LB}}^{fso}\right)}\right] \\ &+ P_{out}^{fso(PL)}\left(\xi_{th_{UB}}^{fso}, \xi_{th_{LB}}^{fso}\right) C_{mix}\left(\xi_{th}^{mix}\right) \\ &+ P_{out}^{rf}\left(\xi_{th}^{mix}\right)\left[1 - P_{out}^{fso(SL)}\left(\xi_{th}^{mix}\right)\right] C_{fso}^{SL}\left(\xi_{th}^{mix}\right), \end{aligned} \tag{34}$$

where $C_{fso}^{PL}(\xi_{th_{UB}}^{fso})$ and $C_{fso}^{PL}(\xi_{th_{LB}}^{fso})$ can be found from (24) by replacing ξ_{th}^{fso} with $\xi_{th_{UB}}^{fso}$ and $\xi_{th_{LB}}^{fso}$, respectively, and all other parameters are already mentioned in Section III-D. The first term in (34) is for

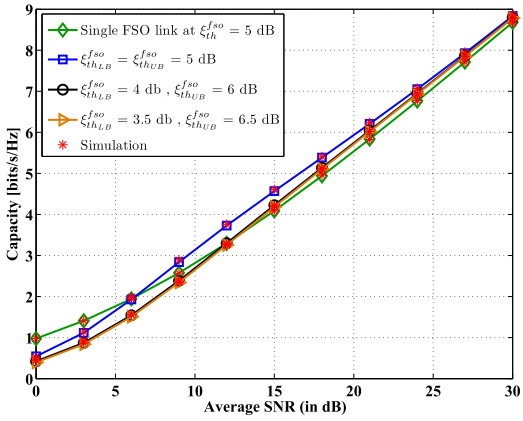

Fig. 10. Average capacity with dual FSO threshold.

the case, $\xi_{fso}^{PL} \geq \xi_{th_{UB}}^{fso}$, when PL is active, while the second term is for the case, $\xi_{th_{LB}}^{fso} \leq \xi_{fso}^{PL} < \xi_{th_{UB}}^{fso}$, rendering PL still to be the chosen path for transmission. If outage occurs in PL, with probability, $P_{out}^{fso(PL)}\left(\xi_{th_{LB}}^{fso}, \xi_{th_{UB}}^{fso}\right)$, SL transmits with capacity $C_{mix}\left(\xi_{th}^{mix}\right)$, as reflected in the third term. Finally, the fourth term accounts for the case when outage occurs at *S-R* link but the *R-D* link is still operational with a capacity $C_{fso}^{SL}\left(\xi_{th}^{mix}\right)$.

As demonstrated in Fig. 10, capacity performance with dual threshold is in general poor (orange/black line) compared to capacity with single threshold (blue line). The cutoff SNR, over which the proposed system exhibits higher capacity than single FSO link (green line), is also higher for dual threshold case. Further, there is negligible effect of difference of thresholds, $\xi_{th_{UB}}^{fso} - \xi_{th_{LB}}^{fso}$, in contrast to outage or BER performances. At high SNR region, however, the behaviour is asymptotic. This is because at high average SNR, PL remains active most of the time, and the system seldom switches to SL.

5. Conclusion and Future Work

In this paper, we presented a FSO/RF-FSO link adaptation scheme for hybrid FSO systems and analyzed its performance. First, we consider a single FSO threshold for switching between links followed by a dual FSO threshold to prevent unnecessary switching. For both the cases, we evaluated different performance metrics like outage probability, average BER, and average capacity. The derived analytical expressions were validated with extensive Monte Carlo simulations. The overall system performance of our proposed hybrid scheme achieves better reliability than the conventional single FSO system. In particular, this hybrid FSO/RF-FSO system demonstrated improved outage and BER performances compared to FSO-only system in all weather conditions.

There are several directions in which the current work may be extended. For example, it would be interesting to study the effect of pointing error in primary/secondary FSO links and the effect of outdated CSI in secondary RF link. Another possibility is to consider secondary links with comparable data rates where the RF link is equipped with massive multiple-input multiple-output (MIMO) capability to match the data rate of FSO links.

Appendix A. Derivation of (13)–(15)

Let, $B^{fso}\left(\xi_{th}^{fso}\right) = \mathcal{I}_1 - \mathcal{I}_2$, where, the first integral,

$$\mathcal{I}_1 = \mathcal{K}_2 \int_0^{\infty} \text{erfc}\left(\sqrt{\xi_{fso}^{PL}/2}\right)\left(\xi_{fso}^{PL}\right)^{\tau_1 - 1} G_{0\,2}^{2\,0}\left[\alpha_t \beta_t \sqrt{\xi_{fso}^{PL}/\bar{\xi}_{fso}^{PL}}\,\middle|\, \begin{matrix} - \\ \frac{\alpha_t - \beta_t}{2}\ \frac{\beta_t - \alpha_t}{2} \end{matrix}\right] \mathrm{d}\xi_{fso}^{PL}, \tag{35}$$

may be solved utilizing [24, eq. (8.4.14.2)] and [25, eq. (21)] to obtain (13). On the other hand, with a simple change of variable, $x = \sqrt{\xi_{fso}/2}$, the second integral,

$$\mathcal{I}_2 = \mathcal{K}_2 \int_0^{\xi_{th}^{fso}} \text{erfc}\left(\sqrt{\xi_{fso}^{PL}/2}\right) \left(\xi_{fso}^{PL}\right)^{\tau_1 - 1} G_{0\,2}^{2\,0}\left[\alpha_t\beta_t\sqrt{\xi_{fso}^{PL}/\bar{\xi}_{fso}^{PL}}\,\middle|\, \tfrac{\alpha_t-\beta_t}{2}\ \tfrac{\beta_t-\alpha_t}{2}\right] \mathrm{d}\xi_{fso}^{PL}, \tag{36}$$

may be expressed with new limits as

$$\mathcal{I}_2 = \mathcal{K}_2 2^{\tau_1+1} \int_0^{\sqrt{\xi_{th}^{fso}/2}} x^{2\tau_1-1}\text{erfc}\,(x)\, G_{0\,2}^{2\,0}\left[\alpha_t\beta_t x\sqrt{2/\bar{\xi}_{fso}^{PL}}\,\middle|\, \tfrac{\alpha_t-\beta_t}{2}\ \tfrac{\beta_t-\alpha_t}{2}\right] \mathrm{d}x. \tag{37}$$

Again, using the exponential series expansion of erfc(·), $\text{erfc}(x) = \frac{1}{6}\exp(-x^2) + \frac{1}{2}\exp\left(-\frac{4}{3}x^2\right)$, we may write, $\mathcal{I}_2 \approx \mathcal{I}_{2_a} + \mathcal{I}_{2_b}$, where

$$\mathcal{I}_{2_a} = \left(\mathcal{K}_2 2_1^{\tau}/3\right) \int_0^{\sqrt{\xi_{th}^{fso}/2}} \exp(-x^2) x^{2\tau_1-1} G_{0\,2}^{2\,0}\left[\alpha_t\beta_t x\sqrt{2/\bar{\xi}_{fso}^{PL}}\,\middle|\, \tfrac{\alpha_t-\beta_t}{2}\ \tfrac{\beta_t-\alpha_t}{2}\right] \mathrm{d}x, \tag{38}$$

and

$$\mathcal{I}_{2_b} = \mathcal{K}_2 2_1^{\tau} \int_0^{\sqrt{\xi_{th}^{fso}/2}} \exp\left(-\frac{4}{3}x^2\right) x^{2\tau_1-1} G_{0\,2}^{2\,0}\left[\alpha_t\beta_t x\sqrt{2/\bar{\xi}_{fso}^{PL}}\,\middle|\, \tfrac{\alpha_t-\beta_t}{2}\ \tfrac{\beta_t-\alpha_t}{2}\right] \mathrm{d}x. \tag{39}$$

Using [29, eq. (1.211.3)] and [25, eq. (27)] in the above equations, we get the simplified expressions as provided in (14) and (15) from (38) and (39), respectively.

Appendix B. Derivation of (17)–(20)

We begin with breaking the term $B^{mix}\left(\xi_{th}^{mix}\right)$ into two separate integrals,

$$B^{mix}\left(\xi_{th}^{mix}\right) = \int_{\xi_{th}^{mix}}^{\infty} P\left(e\middle|\xi_{mix}\right) f_{\xi_{mix}}\left(\xi_{mix}\right) \mathrm{d}\xi_{mix} = \mathcal{I}_3 + \mathcal{I}_4, \tag{40}$$

where

$$\mathcal{I}_3 = \left(\mathcal{K}_1/2\right) \int_{\xi_{th}^{mix}}^{\infty} \text{erfc}\left(\sqrt{\xi_{mix}/2}\right) \xi_{mix}^{\tau_1-1} \exp\left(-\xi_{mix}/\bar{\xi}_{mix}\right) G_{1\,6}^{6\,0}\left[\omega\xi_{mix}\middle|_{1-\tau_1,\mathcal{P}}^{-\tau_1}\right] \mathrm{d}\xi_{mix}, \tag{41}$$

and

$$\mathcal{I}_4 = \mathcal{K}_1/(2\bar{\xi}_{mix}) \int_{\xi_{th}^{mix}}^{\infty} \text{erfc}\left(\sqrt{\xi_{mix}/2}\right) \xi_{mix}^{\tau_1} \exp\left(-\xi_{mix}/\bar{\xi}_{mix}\right) G_{0\,5}^{5\,0}\left[\omega\xi_{mix}\middle|_{\mathcal{P}}^{-}\right] \mathrm{d}\xi_{mix}. \tag{42}$$

Now, using the same exponential series expansion of erfc(·) as used in Appendix A, we may write $\mathcal{I}_3$ as

$$\begin{aligned}\mathcal{I}_3 \approx \left(\mathcal{K}_1/2\right) &\int_{\xi_{th}^{mix}}^{\infty} \left[(1/6)\exp\left(-\xi_{mix}^2/2\right) + (1/2)\exp\left(-4\xi_{mix}^2/3\right)\right] \xi_{mix}^{\tau_1-1} \\ &\times \exp\left(-\xi_{mix}/\bar{\xi}_{mix}\right) G_{1\,6}^{6\,0}\left[\omega\xi_{mix}\middle|_{1-\tau_1,\mathcal{P}}^{-\tau_1}\right] \mathrm{d}\xi_{mix} = \mathcal{I}_{3_a} + \mathcal{I}_{3_b},\end{aligned} \tag{43}$$

where

$$\mathcal{I}_{3_a} = \left(\mathcal{K}_1/12\right) \int_{\xi_{th}^{mix}}^{\infty} \xi_{mix}^{\tau_1-1} \exp\left\{-\xi_{mix}\left(1/\bar{\xi}_{mix} + 1/2\right)\right\} G_{1\,6}^{6\,0}\left[\omega\xi_{mix}\middle|_{1-\tau_1,\mathcal{P}}^{-\tau_1}\right] \mathrm{d}\xi_{mix}, \tag{44}$$

and

$$\mathcal{I}_{3_b} = \left(\mathcal{K}_1/4\right) \int_{\xi_{th}^{mix}}^{\infty} \xi_{mix}^{\tau_1-1} \exp\left\{-\xi_{mix}\left(1/\bar{\xi}_{mix} + 2/3\right)\right\} G_{1\,6}^{6\,0}\left[\omega\xi_{mix}\middle|_{1-\tau_1,\mathcal{P}}^{-\tau_1}\right] \mathrm{d}\xi_{mix}. \tag{45}$$

Now, changing the limit of the above equation and after some mathematical manipulations using [24, eq. (2.24.3.1)] and [25, eq. (26)], we obtain the solutions given in (17) and (18). Following the

same approach for $\mathcal{I}_4$ in (42), we end up with two integrals, i.e. $\mathcal{I}_4 = \mathcal{I}_{4_a} + \mathcal{I}_{4_b}$, which results in the expressions as given in (19) and (20), respectively.

Appendix C. Derivation of (25)–(26)

The two components of $C_{fso}^{PL}\left(\xi_{th}^{fso}\right)$ are $\mathcal{I}_5$ and $\mathcal{I}_6$, and the first component

$$\mathcal{I}_5 = \frac{\mathcal{K}_1}{\ln(2)} \int_0^{\infty} \ln\left(1+\xi_{fso}^{PL}\right) \left(\xi_{fso}^{PL}\right)^{\tau_1 - 1} G_{0\,2}^{2\,0}\left[(\alpha_t\beta_t)\sqrt{\xi_{fso}^{PL}/\bar{\xi}_{fso}^{PL}}\Big|_{\frac{\beta_t-\alpha_t}{2}-\frac{\beta_t-\alpha_t}{2}}\right] \mathrm{d}\xi_{fso}^{PL}, \tag{46}$$

can be deduced to (25) using [25, eq. (11)] and [24, eq. (2.24.1.1)]. On the other hand, the second component

$$\mathcal{I}_6 = \frac{\mathcal{K}_1}{\ln(2)} \int_0^{\xi_{th}^{fso}} \ln\left(1+\xi_{fso}^{PL}\right) \left(\xi_{fso}^{PL}\right)^{\tau_1 - 1} G_{0\,2}^{2\,0}\left[(\alpha_t\beta_t)\sqrt{\xi_{fso}^{PL}/\bar{\xi}_{fso}^{PL}}\Big|_{\frac{\beta_t-\alpha_t}{2}-\frac{\beta_t-\alpha_t}{2}}\right] \mathrm{d}\xi_{fso}^{PL}, \tag{47}$$

can be expressed as in (26) using the Taylor series expansion [24, eq. (45)], $\ln(1+x) = \sum_{n=1}^{\infty} (-1)^{n+1} x^n/n!$.

Appendix D. Derivation of (28)–(31)

The Taylor series expansion, $\ln(1+x) = \sum_{n=1}^{\infty}(-1)^{n+1}x^n/n!$, can be used to obtain

$$\begin{aligned} C_{mix}\left(\xi_{th}^{mix}\right) = {} & \frac{\mathcal{K}_1}{\ln(2)} \sum_{n=1}^{\infty} \frac{(-1)^{n+1}}{n} \int_{\xi_{th}^{mix}}^{\infty} \xi_{mix}^{n+\tau_1-1} \exp\left(-\frac{\xi_{mix}}{\bar{\xi}_{mix}}\right) G_{1\,6}^{6\,0}\left[\omega\xi_{mix}\Big|_{1-\tau_1\mathcal{P}}^{-\tau_1}\right] \mathrm{d}\xi_{mix} \\ & + \frac{\mathcal{K}_1}{\ln(2)\,\bar{\xi}_{mix}} \sum_{n=1}^{\infty} \frac{(-1)^{n+1}}{n} \int_{\xi_{th}^{mix}}^{\infty} \xi_{mix}^{n+\tau_1} \exp\left(-\frac{\xi_{mix}}{\bar{\xi}_{mix}}\right) G_{0\,5}^{5\,0}\left[\omega\xi_{mix}\Big|_{\mathcal{P}}\right] \mathrm{d}\xi_{mix}, \end{aligned} \tag{48}$$

from (27).

Now, expressing the integral interval as a difference, the above equation can be expressed as $C_{mix}\left(\xi_{th}^{mix}\right) = (\mathcal{C}_1 - \mathcal{C}_2) + (\mathcal{C}_3 - \mathcal{C}_4)$. The first integral,

$$\mathcal{C}_1 = \frac{\mathcal{K}_1}{\ln(2)} \sum_{n=1}^{\infty} \frac{(-1)^{n+1}}{n} \int_0^{\infty} \xi_{mix}^{n+\tau_1-1} \exp\left(-\frac{\xi_{mix}}{\bar{\xi}_{mix}}\right) G_{1\,6}^{6\,0}\left[\omega\xi_{mix}\Big|_{1-\tau_1\mathcal{P}}^{-\tau_1}\right] \mathrm{d}\xi_{mix}. \tag{49}$$

is solved with the help of [39, eq. (2.24.3.1)] to obtain (28). Next, using the series, $\exp(-\xi_{mix}/\bar{\xi}_{mix}) = \sum_{n=1}^{\infty}(-1)^k(\xi_{mix}/\bar{\xi}_{mix})^k/k!$ [29, eq. (1.211.3)], the second term,

$$\mathcal{C}_2 = \frac{\mathcal{K}_1}{\ln(2)} \sum_{n=1}^{\infty} \frac{(-1)^{n+1}}{n} \int_0^{\xi_{th}^{mix}} \xi_{mix}^{n+\tau_1-1} \exp\left(-\frac{\xi_{mix}}{\bar{\xi}_{mix}}\right) G_{1\,6}^{6\,0}\left[\omega\xi_{mix}\Big|_{1-\tau_1\mathcal{P}}^{-\tau_1}\right] \mathrm{d}\xi_{mix}. \tag{50}$$

may be resolved into (29). In a similar fashion, the rest of the integrals,

$$\mathcal{C}_3 = \frac{\mathcal{K}_1}{\ln(2)\,\bar{\xi}_{mix}} \sum_{n=1}^{\infty} \frac{(-1)^{n+1}}{n} \int_0^{\infty} \xi_{mix}^{n+\tau_1} \exp\left(-\frac{\xi_{mix}}{\bar{\xi}_{mix}}\right) G_{0\,5}^{5\,0}\left[\omega\xi_{mix}\Big|_{\mathcal{P}}\right] \mathrm{d}\xi_{mix}, \tag{51}$$

and

$$\mathcal{C}_4 = \frac{\mathcal{K}_1}{\ln(2)\,\bar{\xi}_{mix}} \sum_{n=1}^{\infty} \frac{(-1)^{n+1}}{n} \int_0^{\xi_{th}^{mix}} \xi_{mix}^{n+\tau_1} \exp\left(-\frac{\xi_{mix}}{\bar{\xi}_{mix}}\right) G_{0\,5}^{5\,0}\left[\omega\xi_{mix}\Big|_{\mathcal{P}}\right] \mathrm{d}\xi_{mix}. \tag{52}$$

can be simplified to (30) and (31), respectively.

References

[1] J. M. Kahn and D. A. Miller, "Communications expands its space," *Nature Photon.*, vol. 11, no. 1, pp. 5–8, Jan. 2017.

[2] M. Alzenad, M. Z. Shakir, H. Yanikomeroglu, and M. S. Alouini, "FSO-based vertical backhaul/fronthaul framework for 5G+ wireless networks," *IEEE Commun. Mag.*, vol. 56, no. 1, pp. 218–224, Jan. 2018.
[3] I. Sousa, M. P. Queluz, and A. Rodrigues, "An efficient visibility prediction framework for free-space optical systems," *Wireless Pers. Commun.*, vol. 96, no. 3, pp. 3483–3498, Oct. 2017.
[4] P. T. Dat *et al.*, "Investigation of suitability of RF signal transmission over FSO links," in *Proc. IEEE HONET*, Nov. 2007, pp. 1–6.
[5] A. Douik, H. Dahrouj, T. Y. Al-Naffouri, and M. S. Alouini, "Hybrid radio/free-space optical design for next generation backhaul systems," *IEEE Trans. Commun.*, vol. 64, no. 6, pp. 2563–2577, Jun. 2016.
[6] G. T. Djordjevic, M. I. Petkovic, A. M. Cvetkovic, and G. K. Karagiannidis, "Mixed RF/FSO relaying with outdated channel state information," *IEEE J. Sel. Areas Commun.*, vol. 33, no. 9, pp. 1935–1948, Sep. 2015.
[7] H. Dahrouj, A. Douik, F. Rayal, T. Y. Al-Naffouri, and M. S. Alouini, "Cost-effective hybrid RF/FSO backhaul solution for next generation wireless systems," *IEEE Wireless Commun.*, vol. 22, no. 5, pp. 98–104, Oct. 2015.
[8] I. S. Ansari, F. Yilmaz, and M. S. Alouini, "On the performance of mixed RF/FSO dual-hop transmission systems," in *Proc. IEEE 78th Veh. Technol. Conf.*, Jun. 2013, pp. 1–5.
[9] E. Zedini, H. Soury, and M. S. Alouini, "On the performance analysis of dual-hop mixed FSO/RF systems," *IEEE Trans. Wireless Commun.*, vol. 15, no. 5, pp. 3679–3689, May 2016.
[10] B. Bag, A. Das, A. Chandra, and C. Bose, "Capacity analysis for Rayleigh/gamma-gamma mixed RF/FSO link with fixed-gain AF relay," *IEICE Trans. Commun.*, vol. E100-B, no. 10, pp. 1747–1757, Oct. 2017.
[11] M. Usman, H. C. Yang, and M.-S. Alouini, "Practical switching-based hybrid FSO/RF transmission and its performance analysis," *IEEE Photon. J.*, vol. 6, no. 5, Oct. 2014, Art. no. 7902713.
[12] A. Abdulhussein, A. Oka, T. T. Nguyen, and L. Lampe, "Rateless coding for hybrid free-space optical and radio-frequency communication," *IEEE Trans. Wireless Commun.*, vol. 9, no. 3, pp. 907–913, Mar. 2010.
[13] W. Zhang, S. Hranilovic, and C. Shi, "Soft-switching hybrid FSO/RF links using short-length raptor codes: Design and implementation," *IEEE J. Sel. Areas Commun.*, vol. 27, no. 9, pp. 1698–1708, Dec. 2009.
[14] L. Kong, W. Xu, L. Hanzo, H. Zhang, and C. Zhao, "Performance of a free-space-optical relay-assisted hybrid RF/FSO system in generalized-distributed channels," *IEEE Photon. J.*, vol. 7, no. 5, Oct. 2015, Art. no. 7903319.
[15] B. M. Schmidt, "A novel outage capacity objective function for optimal performance monitoring and predictive fault detection in hybrid free-space optical and RF wireless networks," *Commun. Netw.*, vol. 5, no. 4, pp. 305–315, Nov. 2013.
[16] E. Zedini, I. S. Ansari, and M. S. Alouini, "Performance analysis of mixed Nakagami-*m* and gamma-gamma dual-hop FSO transmission systems," *IEEE Photon. J.*, vol. 7, no. 1, Feb. 2015, Art. no. 7900120.
[17] J. Zhang, L. Dai, Y. Zhang, and Z. Wang, "Unified performance analysis of mixed radio frequency/free-space optical dual-hop transmission systems," *J. Lightw. Technol.*, vol. 33, no. 11, pp. 2286–2293, Jun. 2015.
[18] X. Zhu and J. M. Kahn, "Free-space optical communication through atmospheric turbulence channels," *IEEE Trans. Commun.*, vol. 50, no. 8, pp. 1293–1300, Aug. 2002.
[19] M. A. Al-Habash, L. C. Andrews, and R. L. Phillips, "Mathematical model for the irradiance probability density function of a laser beam propagating through turbulent media," *Opt. Eng.*, vol. 40, no. 8, pp. 1554–1562, Aug. 2001.
[20] D. T. Wayne, R. L. Phillips, L. C. Andrews, T. Leclerc, P. Sauer, and J. Stryjewski, "Comparing the log-normal and gamma-gamma model to experimental probability density functions of aperture averaging data," *Proc. SPIE*, vol. 7814, Aug. 2010, pp. 78 140K-1–78 140K-13.
[21] I. S. Ansari, M. S. Alouini, and F. Yilmaz, "On the performance of hybrid RF and RF/FSO fixed gain dual-hop transmission systems," in *Proc. IEEE Saudi Int. Electron., Commun. Photon. Conf.*, Apr. 2013, pp. 1–6.
[22] M. Uysal and J. T. Li, "Error rate performance of coded free-space optical links over gamma-gamma turbulence," in *Proc. IEEE Int. Conf. Commun.* Jun. 2004, vol. 6, pp. 3331–3335.
[23] A. K. Majumdar, "Free-space laser communication performance in the atmospheric channel," in *Free-Space Laser Communications: Principles and Advances* (Series Optical and Fiber Communications Reports), vol. 2, A. K. Majumdar and J. C. Ricklin, Eds. New York, NY, USA: Springer, 2008, pp. 57–108.
[24] A. P. Prudnikov, Y. A. Brychkov, and O. I. Marichev, *Integrals and Series: More Special Functions*, vol. 3. Amsterdam, The Netherlands: Gordon and Breech, 1990.
[25] V. S. Adamchik and O. I. Marichev, "The algorithm for calculating integrals of hypergeometric type functions and its realization in REDUCE system," in *Proc. ACM Int. Symp. Symbolic Algebraic Comput.*, Jul. 1990, pp. 212–224.
[26] A. Chandra, S. Biswas, B. Ghosh, N. Biswas, G. Brante, and R. D. Souza, "Energy efficient relay placement in dual hop 802.15.4 networks," *Wireless Pers. Commun.*, vol. 75, no. 4, pp. 1947–1967, Apr. 2014.
[27] M. O. Hasna and M. S. Alouini, "A performance study of dual-hop transmissions with fixed gain relays," *IEEE Trans. Wireless Commun.*, vol. 3, no. 6, pp. 1963–1968, Nov. 2004.
[28] M. K. Simon and M. S. Alouni, *Digital Communication Over Fading Channels*, 2nd ed. New York, NY, USA: Wiley, 2005.
[29] I. S. Gradshteyn and I. M. Ryzhik, *Table of Integrals, Series, and Products*, 6th ed. San Diego, CA, USA: Academic, 2000.
[30] A. Chaaban, J. M. Morvan, and M. S. Alouini, "Free-space optical communications: Capacity bounds, approximations, and a new sphere-packing perspective," *IEEE Trans. Commun.*, vol. 64, no. 3, pp. 1176–1191, Mar. 2016.